Self-assembled axicon lens in integrated optical fiber

CHRISTOPHER HOLMES,* PETER G R SMITH

Optoelectronics Research Centre, University of Southampton, Southampton, SO17 1BJ, UK
**Corresponding author: christopher.holmes@southampton.ac.uk*

Received XX Month XXXX; revised XX Month, XXXX; accepted XX Month XXXX; posted XX Month XXXX (Doc. ID XXXXX); published XX Month XXXX

This work reports the fabrication of an integrated axicon lens within a monolithic fibre-upon-planar format. The lens is self-assembled around a tapered optical fibre during flame hydrolysis planarization. The formed lens approximates an oblate axicon that upon launch generates a quasi-Bessel beam, guided in the planar optical layer of the substrate. Experimental observations are theoretically concurred using Fourier-based beam propagation.

OCIS codes: *(130.0130) Integrated Optics; (230.7400) Waveguides, slab; (060.2310) Fiber optics.*

http://dx.doi.org/10.1364/OL.99.099999

Bessel light modes have the physical characteristic of diffraction immunity [8,9], a property that has utilization in a diverse range of applications, including optical traps [3–5]; optical coherence tomography [6,7] and nonlinear physics [8,9]. It is widely understood that such beams can be physically realized through use of an axicon, which acts to create a linear phase retardation in the direction transverse to the optical axis [10]. Beams emanating from particularly designed axicons are termed 'non-diffracting', which in reality are only of discreet distance due to energy conservation arguments.

Commonly, axicon lenses have an obtuse apex, but acute angled axicons have also been reported. A recent theoretical study by Khonina et al classifies a family of beam types arising from a range of apex angled axicons [11]. The formation of a quasi-Bessel beam occurs specifically when the half apex angle is greater than the incident angle for the condition of total internal reflection, illustrated in Figure 1 (a). For apex angles smaller in magnitude the diffracting beams that emerge can be classified as: evanescent hollow; evanescent at tip; halo and hollow respectively [11]. For acute angled axicons classification is defined as collimated, focused and hollow beams. This latter classification is cyclical with respect to the number of internal reflections made [12], schematically illustrated for the case of one internal reflection in Figure 1 (b)-(d).

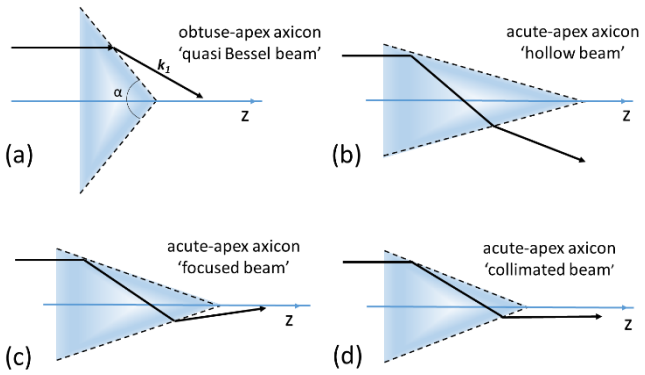

Fig. 1. Schematic illustration of ray paths for axicon lenses, including (a) obtuse apex-angle; (b) – (c) acute apex axicon with single internal reflection.

This Letter reports the self-assembly of an integrated micron-scale oblate axicon refractive lens. This sits within a special class of axicons termed 'micro-axicon', an area that has gained increasing interest, with lens demonstrations upon planar [13], fibre [14,15] and bulk material [16]. The fabrication approach reported is unique and effectively forms two concatenated axicons, the first with an acute apex, formed by a tapered optical fibre and the second with an obtuse apex formed at the distal end of the fibre. The distal lens is fabricated primarily through a self-assembly.

The fabrication method reported monolithically attaches an optical fibre to an optical planar substrate through use of consolidated high purity glass soot. The soot is deposited via Flame Hydrolysis Deposition (FHD), which can manipulate refractive index, stress and thickness of the resulting glass through mass flow controllers. So far the platform, termed Integrated Optical Fibre (IOF) has demonstrated environmental stability [17], physical monitoring [18,19] and refractometry [20,21]. This work expands applications much further, by demonstrating for the first time direct transitional coupling of optical power from the fibre constituent to its planar constituent, opening up new avenues of research and development of the platform. This

could, for example, enable a route for ruggedized connectorisation of silica fibre to silica planar platforms.

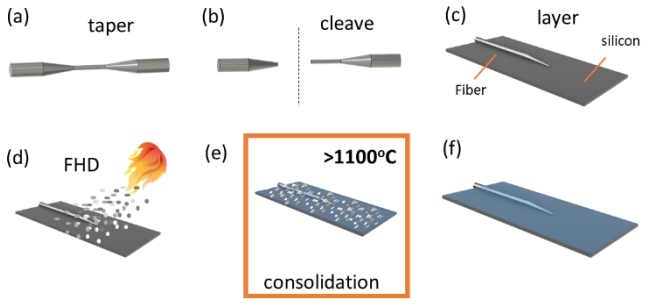

Fig. 2. A schematic illustration shown consecutive steps (a) to (f) of Integrated Optical Fiber fabrication and self-assembly of the axicon lens.

Figure 2 illustrates the process used for component fabrication in this work. It begins by linearly tapering an optical fibre, SMF-28e, to a diameter of 10 µm, using a micro-heater assembly. The optical fibre is subsequently placed upon a single side polished silicon wafer with a 15 µm thermally grown oxide. The oxide layer acts principally as an optical buffer (underclad) between the FHD and silicon. The FHD process uses a torch with four sheath flows. Through the central input flows chloride based precursors, namely PCl_3, BCl_3 and $GeCl_4$, at rates of 100, 80 and 100 sccm respectively. The precursors enter a hydrogen and oxygen flame with flow rates of 5.4 l/min and 2.7 l/min respectively. The flame is shaped using a single argon sheath of flow 8.0 l/min. After deposition the resulting soot was consolidated in a furnace that was ramped in temperature at a rate of 5°C/min to 1360°C and then cooled at a rate of equal magnitude. The high temperature FHD consolidation step occurs >1100°C, Figure 2 (e). This promotes the self-assembly of a lens at the distal end of the tapered fibre and integrates the taper to the planar layer. The lens is self-formed through meniscus effects in the consolidated FHD soot that are subsequently 'frozen-in' when the device is returned to room temperature, observable in Figure 3. The properties of the formed lens depend upon: the diameter of the optical fiber; thickness of glass deposited and composition of the soot (which affect its fluidic behavior, e.g. viscosity and surface tension). This enables a wide range of design freedom.

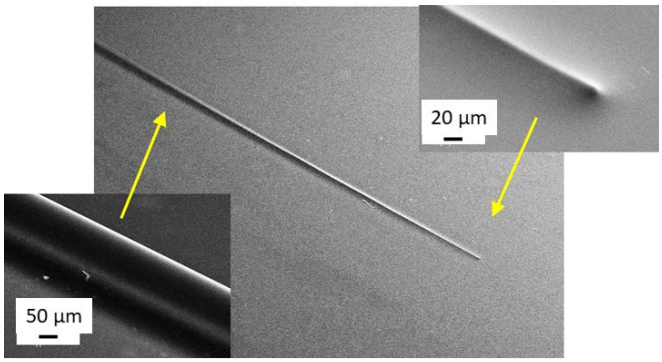

Fig. 3. Scanning electron micrograph images of the attached optical fibre, showing distal end of the fiber, with a self-assembled lens.

After consolidation, the thickness and refractive index of the resultant FHD glass layers was measured using a prism coupler (Metricon). The thickness was taken as 6.10 ± 0.05 µm and refractive index of 1.4516 ± 0.0001 (at 1.553 µm wavelength) and 1.4533 ± 0.0001 (a 633 nm wavelength). The topology of the consolidated surface was analyzed using a stylus profiler (KLA Tencor P16+), illustrated in Figure 4. The apex angle, α, for the distal lens can be approximated as 113.9°. It should also be noted that the optical fiber itself forms an 'acute axicon lens' with an angle of 0.08°, as shown in Figure 4 (a).

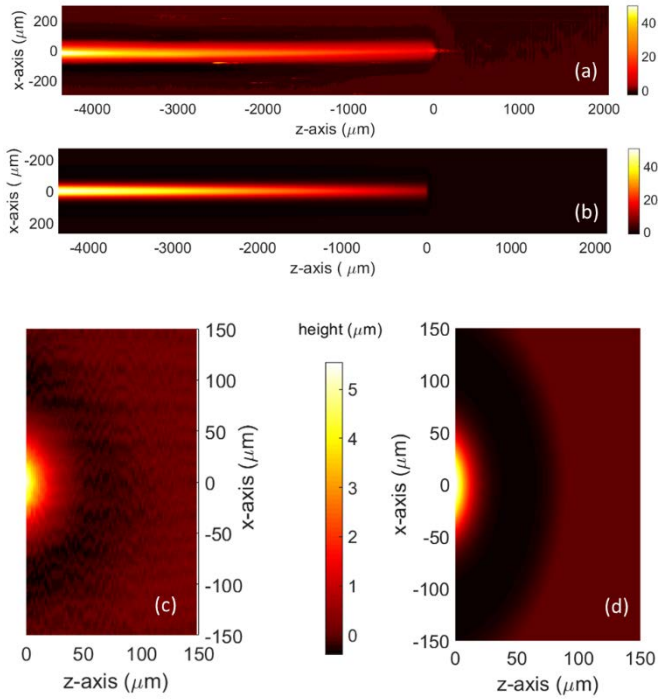

Fig. 4. Profilometry of the attached optical fibre, showing the topology of (a) the acute angled axicon formed by the tapered fibre and (c) the distal end of the fibre with a self-assembled lens, formed from consolidated FHD glass. Analytical approximation for the topology is shown in (b) and (d) respectively.

From Figure 4 it is noted that frozen-in surface tension features result in a trench around the optical fibre, where material is 'pulled in' during consolidation. As expected, trench depth is a function of fibre diameter, principally of the order 0.4 µm in depth.

To observe guidance in the planar layer of the chip, a thin (30 nm) layer of gold was deposited on the top surface. This enabled a plasmon-hybrid mode [22] to be supported as a TM modal solution in the planar layer. Light was launched into the optical fibre from a superluminescent-LED (centered on 780nm). The observed diffraction pattern into the planar layer was captured from above using a complementary metal-oxide semiconductor (CMOS) camera (IDS UI-1240ML_NIR). It should be noted that this technique is non-destructive and through investigating different gold coverages it was concluded that the presence of the gold layer itself had negligible influence on beam output, other

than associated ohmic losses expected that limited the extent of propagation.

The output captured in Figure 5 shows a characteristic central beam and two accompanying spatial side beams that are angularly offset from the optical axis by 13°. Modulation in intensity is also observed, with a period of approximately 115 µm. It is should be noted that such a feature is characteristic of a Bessel-like beam formed by an oblate axicon [10], understood to result from a co-propagating wavevector along the optical axis. Here, the obtuse oblate axicon is formed at the distal end of the fibre. The spatial sideband features are characteristic of an acute apex axicon forming a focused beam [16], consistent with the form of the linear tapered optical fibre.

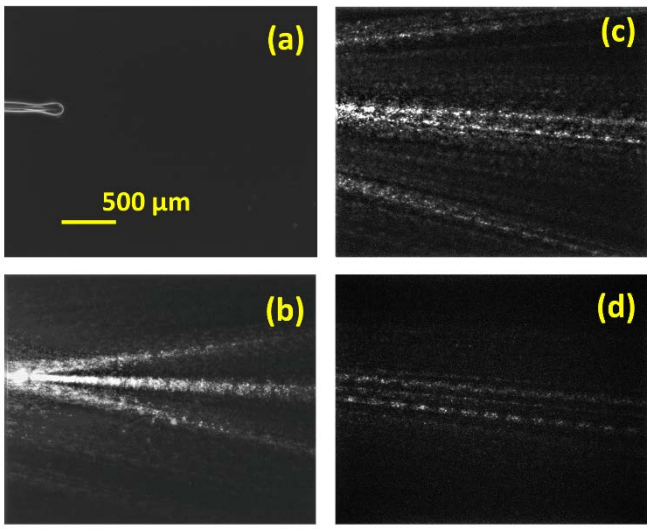

Fig. 5. Images from CMOS camera taken (a) prior to launch (b) upon launch at the distal end of the fibre (b) upon launch at 3 mm offset upon the optical axis (d) upon a 6 mm offset (scale for all images equivalent).

There are several approaches reported to model non-idealized axicons. Hankel transforms are one such approach [10], that are essentially two dimensional circularly symmetric Fourier transforms, utilisable due to the typical rotational symmetry of an axicon. However, due to design complexity for this planar arrangement, a full three dimensional Fourier based beam propagation method was used to model system output. The simulation utilized a Fast Fourier Transform Beam Propagation Method (FFT-BPM) with Perfectly Matched Layers (PMLs) for boundary conditions. The measured topology of the device was analytically approximated for the simulation, as shown in Figure 4. The simulation did not include the thin gold layer that was used to observe the emerging beam, as it was experimentally verified that the presence of the gold does not alter the form of the emerging beam.

Figure 6 depicts the simulated modal power distribution just before light enters the distal lens. For clarity the silicon, thermal oxide, FHD and fibre layers have been marked. It is clear from the simulation that this particular geometry has power leakage, principally into the silicon substrate below and laterally into the planar FHD layer, indicated in the image with arrows showing direction of power flow. Leakage is occurring for two reasons. Firstly, after tapering the power in the fibre guides principally in the cladding layer of the fibre. As the FHD has a higher refractive index power leaks laterally but is partially contained by the self-assembled trench, previously discussed. Furthermore, the fibre cladding and the oxide buffer layer are comparable in refractive index, meaning that power is able to leak into the oxide layer and in turn the silicon. Future geometries that could reduce or remove such effects may include for example development of an initial FHD layer that is lower in refractive index than the optical fibre clad and can be used in place of the thermal oxide.

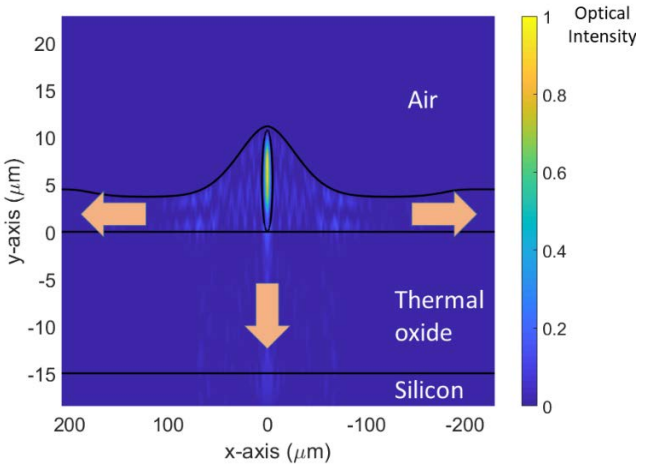

Fig. 6. Cross-sectional view of a three dimensional FFT-BPM, showing the modal intensity just before light enters the integrated lens. Arrows indicate directional flow of power.

Figure 7 is a top view simulation of light propagation from the distal lens and is comparable to the empirical data captured in Figure 5. To achieve the image power was integrated over a 4 µm spatial thickness in proximity to the device surface. Several features are common in both simulated and experimental data, including an intensity undulation, central power distribution and two spatial side band features. Deviations do occur between the simulation observed, due in part to differences between approximated and actual form. Consistent with mechanisms proposed the central and side band features were primarily influenced by the distal lens and fibre taper respectively.

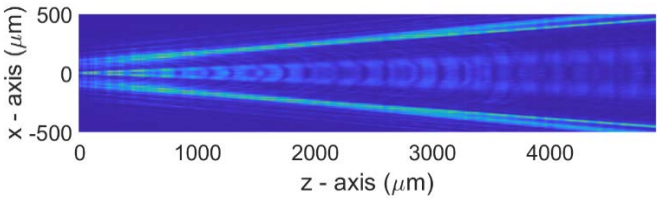

Fig. 7. Three dimensional FFT-BPM showing the intensity distribution after the integrated lens.

This work demonstrates, for the first time, power coupling from an optical fibre to an IOF platform. This is achieved through self-assembly around an optical fibre, forming structures that approximate axicons. Through a non-destructive approach gold deposition approach the optical propagation in the fabricated device was imaged.

Here we enable future integrated applications monolithically combining and coupling light effectively into integrated components within the planar substrate.

Funding

Engineering and Physical Sciences Research Council (EPSRC) UK Quantum Technology Hub for Sensors and Metrology (EP/M013294/1); Air Force Office of Scientific Research (FA9550-16-1-0531);

Acknowledgments

Authors are thankful to Prof. Gilberto Brambilla and Dr Muhammad Imran Mustafa Abdul for provision of tapered optical fibre.

References

1. J. Durin, J. J. Miceli, and J. Eberly, Phys. Rev. Lett. **58**, 1499–1501 (1987).
2. J. Durnin, J. Opt. Soc. Am. A **4**, 651 (1987).
3. I. Manek, Y. B. Ovchinnikov, and R. Grimm, Opt. Commun. **147**, 67–70 (1998).
4. D. G. Grier, Nature **424**, 810–816 (2003).
5. S. Cabrini, C. Liberale, D. Cojoc, a. Carpentiero, M. Prasciolu, S. Mora, V. Degiorgio, F. De Angelis, and E. Di Fabrizio, Microelectron. Eng. **83**, 804–807 (2006).
6. K.-S. Lee and J. P. Rolland, Opt. Lett. **33**, 1696 (2008).
7. Z. Ding, H. Ren, Y. Zhao, J. S. Nelson, and Z. Chen, Opt. Lett. **27**, 243–245 (2002).
8. T. Wulle and S. Herminghaus, Phys. Rev. Lett. **71**, 209–209 (1993).
9. P. Johannisson, D. Anderson, M. Lisak, and M. Marklund, Opt. Commun. **222**, 107–115 (2003).
10. O. Brzobohatý, T. Cizmár, and P. Zemánek, Opt. Express **16**, 12688–12700 (2008).
11. S. Khonina, S. Degtyarev, D. Savelyev, and A. Ustinov, Opt. Express **25**, 19052 (2017).
12. A. V. Ustinov and S. N. Khonina, Opt. Mem. Neural Networks **21**, 133–144 (2012).
13. H. Kurt, J. Opt. Soc. Am. B **26**, 981 (2009).
14. K. Bachus, E. S. de L. Filho, K. Wlodarczyk, R. Oleschuk, Y. Messaddeq, and H.-P. Loock, Opt. Express **24**, 20346 (2016).
15. H. Melkonyan, K. Sloyan, K. Twayana, P. Moreira, and M. S. Dahlem, IEEE Photonics J. **9**, (2017).
16. S. Gorelick and A. De Marco, Opt. Express **26**, 32324–32331 (2018).
17. S. G. Lynch, C. Holmes, S. A. Berry, J. C. Gates, A. Jantzen, T. I. Ferreiro, and P. G. R. Smith, Opt. Express **24**, 22781–22788 (2016).
18. C. Holmes, J. C. Gates, and P. G. R. Smith, Opt. Express **22**, 32150 (2014).
19. C. Holmes, A. Jantzen, A. C. Gray, L. G. Carpenter, P. C. Gow, S. G. Lynch, J. C. Gates, and P. G. R. Smith, IEEE Sens. J. **17**, 6960–6965 (2017).
20. C. Holmes, A. Jantzen, A. C. Gray, P. C. Gow, L. G. Carpenter, R. H. S. Bannerman, J. C. Gates, and P. G. R. Smith, Opt. Lett. **43**, 791–794 (2018).
21. A. C. Gray, A. Jantzen, P. C. Gow, D. H. Smith, C. B. E. Gawith, P. G. R. Smith, and C. Holmes, Opt. Express **26**, 9155–9164 (2018).
22. R. Kashyap and G. Nemova, J. Sensors **2009**, 1–9 (2009).

References – with title.

1. J. Durin, J. J. Miceli, and J. Eberly, "Diffraction-Free Beams," Phys. Rev. Lett. **58**, 1499–1501 (1987).
2. J. Durnin, "Exact solutions for nondiffracting beams I The scalar theory," J. Opt. Soc. Am. A **4**, 651 (1987).
3. I. Manek, Y. B. Ovchinnikov, and R. Grimm, "Generation of a hollow laser beam for atom trapping using an axicon," Opt. Commun. **147**, 67–70 (1998).
4. D. G. Grier, "A revolution in optical manipulation," Nature **424**, 810–816 (2003).
5. S. Cabrini, C. Liberale, D. Cojoc, a. Carpentiero, M. Prasciolu, S. Mora, V. Degiorgio, F. De Angelis, and E. Di Fabrizio, "Axicon lens on optical fiber forming optical tweezers, made by focused ion beam milling," Microelectron. Eng. **83**, 804–807 (2006).
6. K.-S. Lee and J. P. Rolland, "Bessel beam spectral-domain high-resolution optical coherence tomography with micro-optic axicon providing extended focusing range," Opt. Lett. **33**, 1696 (2008).
7. Z. Ding, H. Ren, Y. Zhao, J. S. Nelson, and Z. Chen, "High-resolution optical coherence tomography over a large depth range with an axicon lens.," Opt. Lett. **27**, 243–245 (2002).
8. T. Wulle and S. Herminghaus, "Nonlinear Optics of Bessel Beams," Phys. Rev. Lett. **71**, 209–209 (1993).
9. P. Johannisson, D. Anderson, M. Lisak, and M. Marklund, "Nonlinear Bessel beams," Opt. Commun. **222**, 107–115 (2003).
10. O. Brzobohatý, T. Cizmár, and P. Zemánek, "High quality quasi-Bessel beam generated by round-tip axicon," Opt. Express **16**, 12688–12700 (2008).
11. S. Khonina, S. Degtyarev, D. Savelyev, and A. Ustinov, "Focused, evanescent, hollow, and collimated beams formed by microaxicons with different conical angles," Opt. Express **25**, 19052 (2017).
12. A. V. Ustinov and S. N. Khonina, "Calculating the complex transmission function of refractive axicons," Opt. Mem. Neural Networks **21**, 133–144 (2012).
13. H. Kurt, "Limited-diffraction light propagation with axicon-shape photonic crystals," J. Opt. Soc. Am. B **26**, 981 (2009).
14. K. Bachus, E. S. de L. Filho, K. Wlodarczyk, R. Oleschuk, Y. Messaddeq, and H.-P. Loock, "Fabrication of axicon microlenses on capillaries and microstructured fibers by wet etching," Opt. Express **24**, 20346 (2016).
15. H. Melkonyan, K. Sloyan, K. Twayana, P. Moreira, and M. S. Dahlem, "Efficient Fiber-to-Waveguide Edge Coupling Using an Optical Fiber Axicon Lens Fabricated by Focused Ion Beam," IEEE Photonics J. **9**, (2017).
16. S. Gorelick and A. De Marco, "Refractive micro-lenses and micro-axicons in single-crystal lithium niobate," Opt. Express **26**, 32324–32331 (2018).
17. S. G. Lynch, C. Holmes, S. A. Berry, J. C. Gates, A. Jantzen, T. I. Ferreiro, and P. G. R. Smith, "External cavity diode laser based upon an FBG in an integrated optical fiber platform," Opt. Express **24**, 22781–22788 (2016).
18. C. Holmes, J. C. Gates, and P. G. R. Smith, "Planarised optical fiber composite using flame hydrolysis deposition demonstrating an integrated FBG anemometer," Opt. Express **22**, 32150 (2014).
19. C. Holmes, A. Jantzen, A. C. Gray, L. G. Carpenter, P. C. Gow, S. G. Lynch, J. C. Gates, and P. G. R. Smith, "Integrated Optical Fiber-tip Cantilevers," IEEE Sens. J. **17**, 6960–6965 (2017).
20. C. Holmes, A. Jantzen, A. C. Gray, P. C. Gow, L. G. Carpenter, R. H. S. Bannerman, J. C. Gates, and P. G. R. Smith, "Evanescent field refractometry in planar optical fiber," Opt. Lett. **43**, 791–794 (2018).
21. A. C. Gray, A. Jantzen, P. C. Gow, D. H. Smith, C. B. E. Gawith, P. G. R. Smith, and C. Holmes, "Leaky mode integrated optical fibre refractometer," Opt. Express **26**, 9155–9164 (2018).
22. R. Kashyap and G. Nemova, "Surface Plasmon Resonance-Based Fiber and Planar Waveguide Sensors," J. Sensors **2009**, 1–9 (2009).